Experimental Investigation of Jet Impingement by Stereo PIV

Hua Wang[1*], Gökhan Ergin[1]

1. Dantec Dynamics A/S, Skovlunde, Denmark
* Corresponding author: hwg@dantecdynamics.com

Abstract
Impinging jets have been studied extensively thanks to their potential in obtaining high convective heat transfer rates in various applications that require intensive heating or cooling. As a first step, a better understanding of the flow field is essential in order to reveal the mechanisms for the enhanced heat transfer rates. For this purpose, a stereo PIV experiment has been performed on a jet impinging on a flat plate at room temperature with a moderate Reynolds number (*Re*=4000). The three-component velocity field is measured in the center plane of the jet using a Stereoscopic PIV system. Finally, a proper orthogonal decomposition (POD) analysis is performed, revealing the modes involved in the process. The POD analysis indicates that the vortical structures sweeping over the flat surface may be the reason for increased convective heat transfer from the surface.

1. Introduction

Impinging jets on a plane surface are frequently used for intensive heating or cooling in various applications [1]. The reason is that impinging jets are known to produce some of the highest Nusselt numbers using single-phase convection in the vicinity of the stagnation/impinging point [2]. As a result, numerous studies have been conducted to reveal the heat transfer characteristics of impinging jets under various conditions, and one of the earliest experimental studies is reported in Reference 3. A summary of generic correlations, including many parameters for both single jets and multiple jet arrays, can be found in Reference 4.

Realizing that the essence of heat transfer enhancement lies in the flow field and turbulent fluid motion, some recent works have focused on measuring both the mean and fluctuating velocities, aiming to provide more information about both the mean flow and turbulence characteristics [1]. Early research used Constant Temperature Anemometry (CTA) or Laser Doppler Anemometry (LDA) to measure the fluctuating velocity components point by point [5]. Recently Particle Image Velocimetry (PIV) and Particle Tracking Velocimetry (PTV) methods are more frequently applied, for simultaneous measurement of 2- or 3-component velocity fields in a plane or in a volume [6-7].

Although numerous velocity measurements have been reported, at various experimental conditions, most measurements are performed to obtain 2-components of the velocity. In order to get a better understanding of the three-dimensional flow field, the acquisition of 3rd velocity component is quite important. Stereoscopic PIV is one of the PIV techniques, which can measure three velocity components in a plane (2D3C) at the same time, based on the principle of parallax [8]. Compared with Volumetric PIV (3D3C), it is much less complex, while still capable of providing 3D information about the flow. In the present work, Stereoscopic PIV measurements are performed on an impinging jet, aiming to unveil detailed information about the flow field. In particular, all of the three velocity components measured in the jet center plane will be presented and analyzed in depth. In addition, a Proper Orthogonal Decomposition (POD) analysis is performed to produce a deeper insight into the flow field dynamics. This has been proved to be a powerful and elegant method to extract the dominant features from the flow field [9].

2. Experimental Setup and data processing

2.1 Flow rig

Figure 1 illustrates the impinging jet flow rig and the stereoscopic imaging setup. The continuous air jet was produced using a blower-type fan, situated well upstream of the nozzle exit. The flow passes through a converging section before the nozzle exit with an internal diameter of D=30mm. Dimensions of the converging section and the nozzle is also given in Figure1 in terms of the nozzle diameter, D. A screen was installed upstream of the converging section to break down larger turbulent structures in the flow. It was observed that

the jet studied in this measurement was not fully developed at the exit of the nozzle, but rather had a near-top-hat profile.

The jet impinged perpendicularly to the center of a square, flat metal plate, with a planar dimension of 10D x 10D, and situated 2.7 D away from the nozzle exit. An orthogonal coordinate system is defined with its origin at the center of the jet exit, is shown in Figure 1. The y-axis is measured along the jet axis and is taken as positive in the jet mean flow direction. The x- and z- coordinate is measured along the jet exit plane.

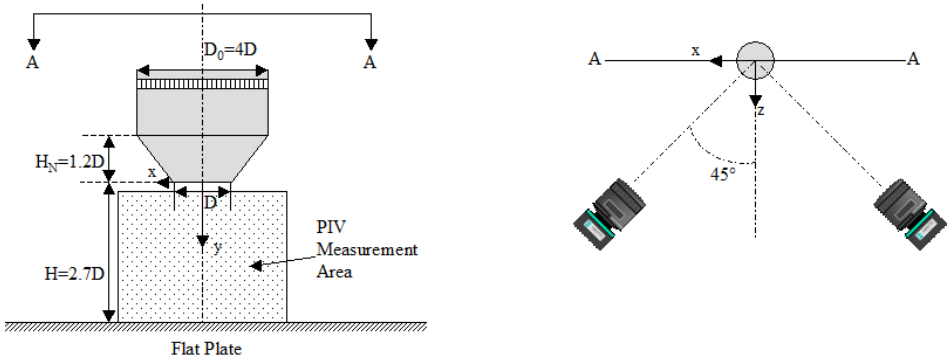

Figure 1 Flow rig and Stereo PIV set up

2.2 Measurement setup

A Dantec Dynamics PIV system is used for the velocity measurements, comprising a DualPower 65-15 Nd:YAG twin cavity laser (max. power per pulse 65 mJ, max. trigger rate15 Hz), two FlowSense EO CCD cameras (2046 x 2046 pixels^2, 12 bit) two Nikkor 60 mm lenses, a Timerbox for the synchronization and DynamicStudio software to control the whole measurement. The angle between the two cameras was set to be 90° and the cameras were symmetric with the z-axis (shown in Figure 1), to achieve the best stereoscopic reconstruction accuracy. Each of the cameras was mounted onto a special mechanical mount to enforce the Scheimpflug condition and thereby achieve well-focused particle images in the whole field of view. The aperture of each lens was set to be f/8 for sufficient SNR for stereo PIV processing. A narrow band pass filter was mounted in front of each camera lens to remove the ambient light. The overlapped Field of View was approximately 100 x 100 mm^2, resulting an image resolution of 70 μm per pixel.

Light sheet optics was mounted at the laser exit to generate a diverging light sheet, passing the center of the jet through x-axis. The light sheet had a width less than 1 mm. The tracer particles were μm-sized olive oil droplets, generated from a liquid atomizer. These droplets were injected into the flow well upstream of the nozzle to ensure uniform seeding with negligible influence on the jet flow downstream.

Double frame images were acquired with pulse separation time of 120 μs and a frequency of 9 Hz. This pulse separation resulted a particle displacement in the jet potential core area as approximately 10 pixels, which is mostly accepted for PIV processing. In total, 1000 image pairs were recorded for statistical analysis.

Each camera was calibrated by capturing still images of a dot-pattern target (100 x 100 mm^2) at seven different z positions (from –3 mm to 3 mm, with 1 mm intervals). The calibration was performed using a 3rd-order polynomial mode [10] and the reprojection error for each camera view was approximately 0.7 pixels.

2.3 Data processing

Adaptive PIV processing routine in DynamicStudio was used to process each image pair. The algorithm is an iterative and adaptive cross-correlation based displacement estimator combined with window shifting, window deformation, and sub-pixel analysis. It iteratively adjusts the size and the shape of the individual interrogation areas (IAs) during processing in order to adapt to local seeding densities and flow gradients. The iteration process started with an IA size 64 x 64 (pixel^2), and ended with an IA size 16 x 16 pixel^2. The grid step size was

set to be 8 x 8, which resulted an overlap of 50%. 15 iterations were carried out for each image pair to achieve sufficient valid vectors; and after each iteration the universal outlier detection [11] was applied in a neighborhood of 5 x 5 vectors.

As the stereoscopic vector reconstruction is very sensitive to measurement errors originating from the 2D2C vector maps from each camera view, sufficient smoothing is often applied before reconstruction. One way of smoothing vector map ensembles is a flow reconstruction using high-energy POD modes with physical meaning, and excluding low-energy POD modes that represent noise. For this purpose, a modal analysis and flow reconstruction is performed using POD. This was followed by another round of universal outlier detection with a neighborhood of 9 x 9 vectors. Then stereo reconstruction was performed, based on the calibration performed previously. Thanks to this process routine, measurement noise was largely reduced and a statistical analysis based on these 1000 stereo PIV dataset can be performed.

3. Results and analysis

3.1 Mean and fluctuation of the velocity field

Figure 2, 3, and 4 give the radial profiles of the mean velocity components; v, u, and w respectively. All of the shown velocities are scaled by the mean jet exit velocity – V_j = 2.25 m/s. The Reynolds number based on the mean jet velocity and the nozzle diameter is computed as *Re* = 4,000. In Figure 2, the velocity profiles at y/D = 0.2 and y/D = 1 show that the jet is still in the developing stage, tending to have a top-hat profile. Inside the jet, the vertical velocity (V) first decreases slowly as the jet moving away from the nozzle, with a slowly increasing deceleration rate. The influence of the plate on the jet velocity is only obvious when the jet is approaching the wall: from y/D = 2 to y/D = 2.6, the velocity is decreased more than 60%.

Different from the trend shown inside the jet, the velocity increases as the measurement line approaching the impinging plate in the area 1<|x/D|<0.5. This is mainly due to the expansion of the jet, in both the jet exit region and impinging region. When |x/D|>1, the vertical velocity is effectively zero, although further away from the jet axis, there is small negative vertical velocity near the impinging plate, indicating the rebounce of the jet. All of these phenomena agree well with earlier measurements [2].

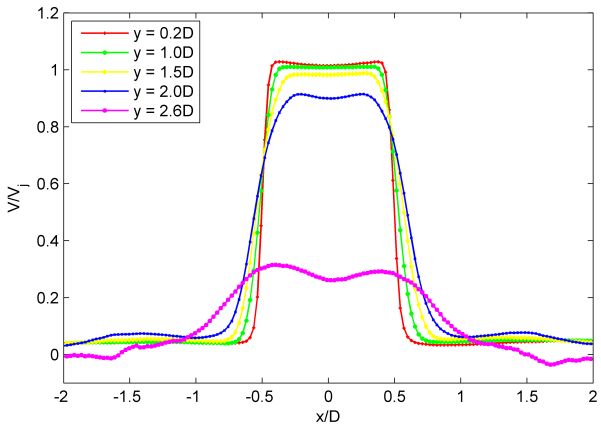

Figure 2 Radial profiles of mean vertical velocity (V) at various distances between the pipe exit and the plate

As can be seen in Figure 3, the radial velocity is effectively very small when y/D<2. Nonetheless, the magnitude of radial velocity still increases slightly as the jet moving away from the nozzle, due to the jet expansion. When the jet reaches the plate, the radial velocity increases dramatically, due to the flow turning away from the stagnation point. The magnitude of the radial velocity near the plate (y/D = 2.6) first increases due to the lateral expansion of the jet, until x/D = 0.6; and then the radial velocity profile decreases, indicating an interaction between the impinging jet and the surrounded air. This also agrees with earlier measurements [2].

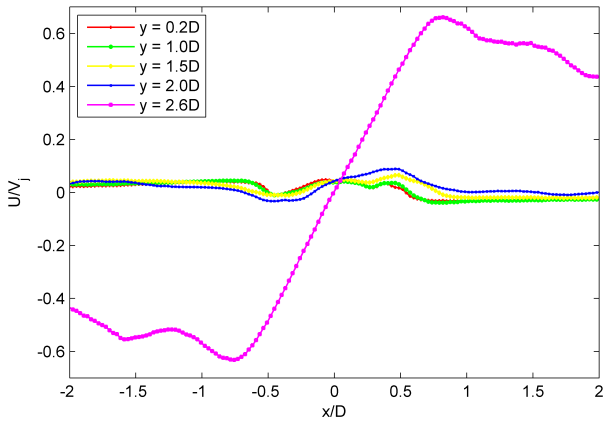

Figure 3 Radial profiles of mean horizontal velocity (U) at various distances between the pipe exit and the plate

As seen in Figure 4, and as expected in the centerplane, the out-of-plane velocity (W) is effectively very small in the entire measurement domain.

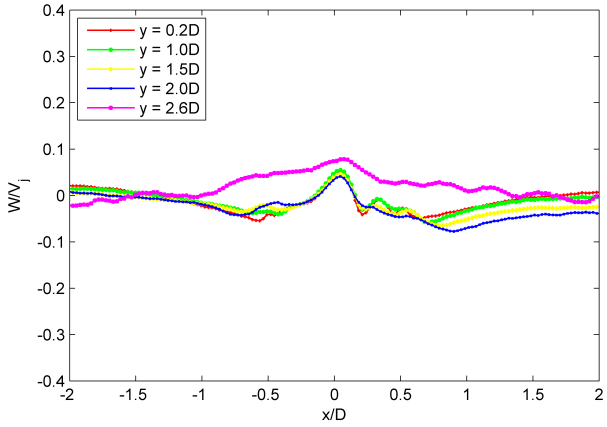

Figure 4 Radial profiles of mean out of plane velocity (W) at various distances between the pipe exit and the plate

Figure 5-7 show the standard deviation (std) of each velocity component at various positions – also scaled by the mean jet exit velocity V_j. The results show similar standard deviation developing trend along all three directions. Inside the jet ($|x/D| \leq 0.5$), the std of each velocity component first increase as the jet moving away from the nozzle, and then decrease when the jet is approaching the plate, due to the stagnation of the flow. At the edge of the jet, it shows max. std for all three velocity components at different y positions, except where the jet approaches the plate. When $|x/D| > 1.2$, the std of all of the velocity components increases in all of the three direction, indicating again the interaction process between the jet and the ambient air. The trend shown here is in good agreement with previous study [2].

It has to be mentioned that although the out-of-plane velocity is effectively very small in the whole field of measurement, its std profile is similar to the std of the other two velocity components. In other words, although the mean crossflow in the centerplane is very small, the measured turbulent fluctuations in this direction have the same order of magnitude and spatial distribution. Additionally, this results of W' presents a monotonic increasing as further away from the jet axis, in the jet impact region, while the fluctuation of other two velocity components are approximately constant outside of the jet (y/D = 2.6). The importance of stereoscopic measurement presents itself here: as a result of the third velocity component measurement, the total turbulence kinetic energy computation is more accurate.

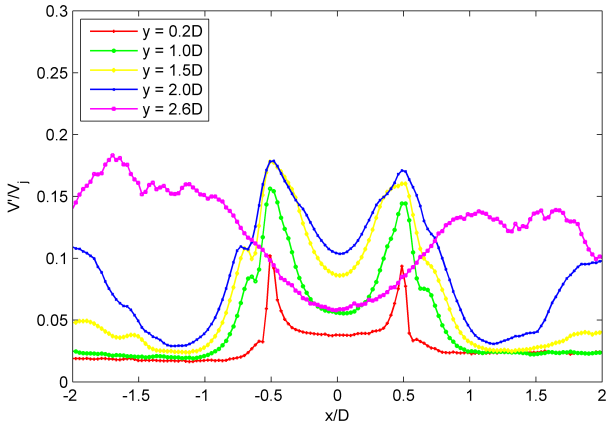

Figure 5 Radial profiles of the standard deviation of vertical velocity (V') at various distances between the pipe exit and the plate

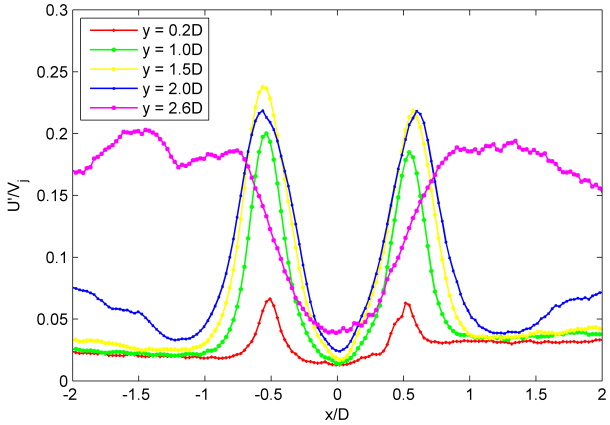

Figure 6 Radial profiles of the standard deviation of horizontal velocity (U') at various distances between the pipe exit and the plate

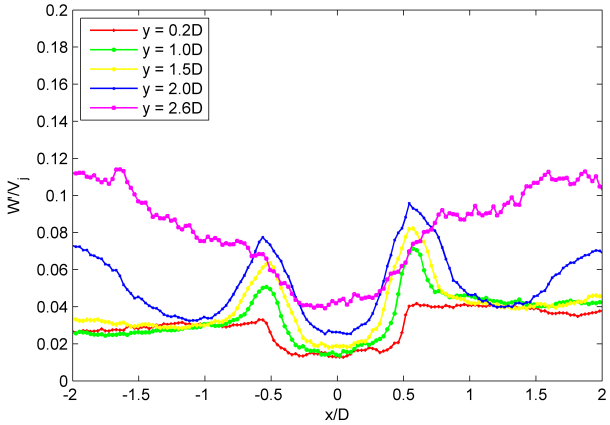

Figure 7 Radial profiles of the standard deviation of out-of-plane velocity (W') at various distances between the pipe exit and the plate

Figure 8 shows the turbulent kinetic energy k spatial distribution, which is defined as:

$$k=(U'^2+V'^2+W'^2)/2 \quad (1)$$

High level of turbulence is only observed in the region where jet is mixed with ambient air. In the stagnation area, the turbulence level is effectively very low, due to the presence of the wall in this region. In the region above the stagnation area, the turbulence level is slightly higher, which is the result of ambient air entrainment into the jet. Above all, the strongest turbulence is observed 0.2 diameters from the plate and around 1.8 diameters away from the jet centerline. This indicates a strong interaction between the wall jet and ambient air.

According to the results of std of different velocity components at different radial profiles (Figure 5-7), the U' and V' are approximately constant outside of the jet, but W' is monotonically increasing in this area. This indicates the start of tangential expansion of the jet.

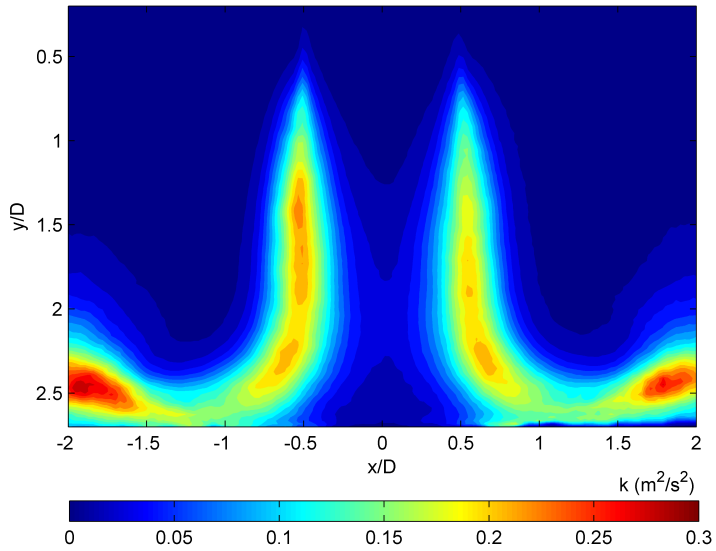

Figure 8 Turbulence kinetic energy distribution

3.2 POD analysis

POD analysis has been performed to expose the high-energy modes in the flow. First a convergence analysis is performed. The POD analysis At first, PODs for different ensemble sizes taken from the same data set were calculated and analyzed with regard to the first 100 modes, to determine the influence of sample size on the turbulent energy distribution. The results indicate a convergence of the spectra once the ensemble size exceeds 800 samples. Consequently, 1000 samples acquired in this study are enough to reveal the dynamics of the flow.

Figure 9 shows the eigen-value spectra of the PODs for the acquired flow field in terms of energy fraction (Figure 9 (a)) and cumulative energy content (Figure 9 (b)). The spectrum exhibits a monotonic decrease of turbulent energy with increasing mode number, indicating no dominance of any periodic elements. In addition, both of the energy fraction plot and the cumulative energy plot show that a considerable number of modes are required to significantly contribute to the total turbulent energy of the flow, although 50% of the fluctuating energy is contained in the first 16 modes.

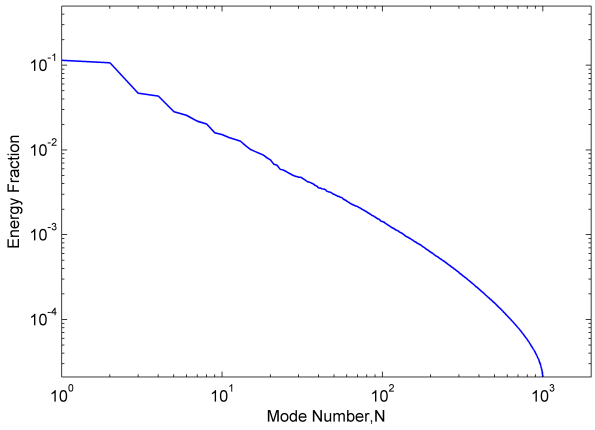

(a)

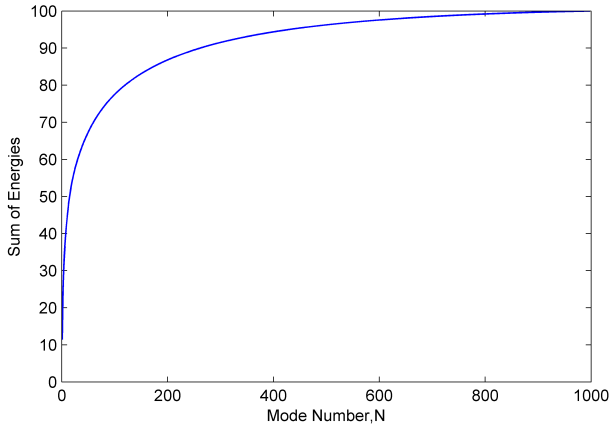

(b)

Figure 9 POD eigen-value spectra for the investigated flow field

Figure 10 shows the spatial projection of the POD basis function for the first 6 modes in the jet center plane. Both the colors and the length of the vectors indicate the velocity magnitude, which is calculated from all three measured velocity components. Nonetheless, it has to be mentioned that the magnitude of out-of-plane velocity (W) is effectively very small in all of the POD modes, and could be considered negligible.

The projection of the first mode shows the mean flow field (Figure 10 (a)). No large vortex structure has been observed here, although large recirculation zone has been reported by [12]. This is primarily because this measurement was focused on the near-field (-2<x/D<2), where wall reflection effects are most significant.

However, various vortex structures can be observed from the projection of higher POD mode numbers. In the region before the jet impinges onto the plate, vortex pairs are can be clearly observed in the second and the third modes. In the followed two modes, the dominant coherent structures are found to be where the jet expands. As the modes number increasing, the dominant vortex is moving from the jet edge to far field, indicating a spatial turbulent energy transfer process: the turbulence is originally brought by the jet to the measurement field. Upstream of the impinging, the turbulence is concentrated on the jet edge, where the vortex ring exists. Here is also where air is entrained into the jet by this vortex. During the impinging, the turbulence is moving along the plate as the jet expanding. Afterwards. The turbulence is transmitted to the ambient.

In addition, a sweeping vortex structure can be observed at each side of the jet from mode 2 to mode 6. In fact, this structure can be also observed in many other lower energy modes, although not presented here. The existence of these structures at different modes proves that the interaction between the impinging jet and the air has a very wide turbulence scale range. This might be also related with the increased convective heat transfer from the surface.

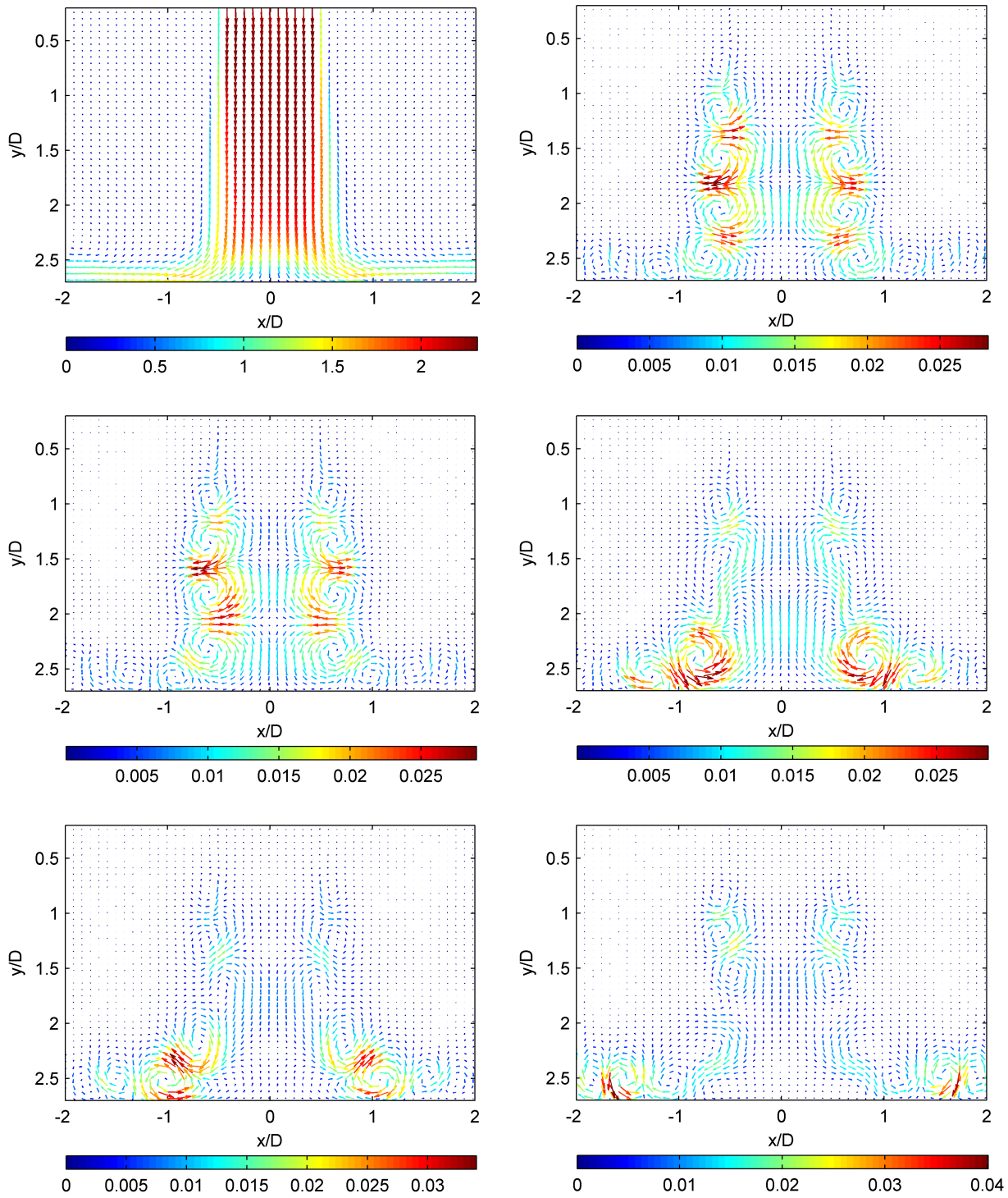

Figure 10 shows the POD projection of each of the first six modes. The first one shows the mean flow field, which contributes slightly more than10% of the total energy

4. Conclusions

The focus of the current study was to investigate the flow field from an impinging jet using stereo PIV measurement. The 3 dimensional velocity field results from an impinging jet of moderate Reynolds number of 4000 is reported at the jet center plane.

The analysis of the time-mean flow field reveals that out of plane velocity is effectively very small, although its fluctuation presents the same developing trend as other two velocity components: the fluctuation of all

three velocity components are larger in the jet edge and near-plate region, where strong interaction between the jet and the ambient happens.

The velocity field was also analyzed by POD, allowing for a detailed insight into the fluid dynamic processes Various modes involved in the process are presented. The results indicate that the vortical structures sweeping over the flat surface may be the reason for increased convective heat transfer from the surface.

References

[1] Geers, F. G., Tummers, M. J. & Hanjalic, G. K. 2004 Experimental investigation of impinging jet arrays. Experiments in Fluids 36, 946-958
[2] Fairweather, M. & Hargrave, G. K. 2002 Experimental investigation of an axisymmetric, impinging turbulent jet. 1. Velocity field. Experiments in Fluids 33, 464-471
[3] Gardon, R. & Akfirat, J. C. 1965 The role of turbulence in determine the heat transfer characteristics of impinging jets. Int. J. Heat Mass Transfer 8, 1261-1272
[4] Martin, H. 1977 Heat and mass transfer between impinging gas jets and solid surfaces. Advances in heat transfer 13, 1-60
[5] Cooper, D., Jackson, D. C., Launder B. E. and Liao G. X. 1993 Impinging jet studies for turbulence model assessment – I. Flow-field experiments. Int. J. Heat mass Transfer 36 (10), 2675-2684
[6] Fairweather, M. & Hargrave, G. K. 2001 DPIV measurements in axisymmetric, impinging turbulent jets. In Processing of the 4th International Symposium on Particle Image Velocimetry, Gottingen, Germany, September 2001
[7] Bilsky, A, Heinz, O., Ilyushin, B., Kaipov, P. & Markovich, D. 2002 PIV measurements with conditional sampling in axisymmetric impinging jet. In: Processing of the 11th International Symposium on Applications of laser Techniques to Fluid Mechanics, Lisbon, Portugal
[8] Adrian, R. J., & Westerweel, J. 2010 Particle image velocimetry. Cambridge University Press.
[9] Schulz, S., Schueren, S. & Wolfersdorf, J. 2014 A particle image velocimetry based investigation of the flow field in an oblique jet impingement configuration. Journal of Turbomachinery 136, 051009-1
[10] Soloff, S. M., Adrian, R. J. & Liu, Z. C. 1997 Distortion compensation for generalized stereoscopic particle image velocimetry. Measurement Science and Technology 8, 1441-1454
[11] Westerweel, J. & Scarano, F. 2005 Universal outlier detection for PIV data. Experiments in Fluids 39, 1096-1100
[12] Dianat, M., Fairweather, M. & Jones, W. P. 1995 Predictions of the concentration field of an impacting turbulent jet. In: Processing of the 10th Symposium on Turbulent Shear Flows 2, Pennsylvania State University, University Park, PA, U.S.A.